JOURNAL OF ENZYME INHIBITION AND MEDICINAL CHEMISTRY, 2017
VOL. 32, NO. 1, 264–270
http://dx.doi.org/10.1080/14756366.2016.1247061

Taylor & Francis
Taylor & Francis Group

RESEARCH ARTICLE

OPEN ACCESS

Through scaffold modification to 3,5-diaryl-4,5-dihydroisoxazoles: new potent and selective inhibitors of monoamine oxidase B

Rita Meleddu[a], Simona Distinto[a], Roberto Cirilli[b], Stefano Alcaro[c], Matilde Yanez[d], Maria Luisa Sanna[a], Angela Corona[a], Claudia Melis[a], Giulia Bianco[a], Peter Matyus[e], Filippo Cottiglia[a] and Elias Maccioni[a]

[a]Department of Life and Environmental Sciences, University of Cagliari, Cagliari, Italy; [b]Dipartimento del Farmaco, Istituto Superiore di Sanità, Rome, Italy; [c]Dipartimento di Scienze della Salute, Università Magna Græcia di Catanzaro, Catanzaro, Italy; [d]Departamento de Farmacología and Instituto de Farmacia Industrial, Universidad de Santiago de Compostela, Campus Universitario Sur, Santiago de Compostela, Spain; [e]Department of Organic Chemistry, Semmelweis University, Budapest, Hungary

ABSTRACT

3,5-Diaryl-4,5-dihydroisoxazoles were synthesized and evaluated as monoamine oxidase (MAO) enzyme inhibitors and iron chelators. All compounds exhibited selective inhibitory activity towards the B isoform of MAO in the nanomolar concentration range. The best performing compound was preliminarily evaluated for its ability to bind iron II and III cations, indicating that neither iron II nor iron III is coordinated. The best compounds racemic mixtures were separated and single enantiomers inhibitory activity evaluated. Furthermore, none of the synthesised compounds exhibited activity towards MAO A. Overall, these data support our hypothesis that 3,5-diaryl-4,5-dihydroisoxazoles are promising scaffolds for the design of neuroprotective agents.

ARTICLE HISTORY
Received 4 August 2016
Revised 5 September 2016
Accepted 5 September 2016

KEYWORDS
3,5-diaryl-dihydroisoxazoles; MAO B selective inhibitors; neuroprotective agents

Introduction

Amine oxidase is a widely diffused family of enzymes responsible for the oxidative deamination of both endogenous and exogenous monoamines, diamines and polyamines. These enzymes are divided into two classes, flavin adenine dinucleotide amino oxidase (FAD-AO) (EC 1.4.3.4)[1] and copper topaquinone amino oxidase (Cu/TPQ-AO)[2]. The former, named monoamine oxidase (MAO), contains flavin adenin dinucleotide (FAD) as a cofactor while the latter contains 2,4,5-trihydroxyphenylalanine quinone as cofactor (TPQ-Cu) and are inhibited by semicarbazide. Regarding FAD-AO, two isoforms, MAO-A and MAO-B, have been isolated, differing from central nervous system (CNS) location, substrate specificity and sensitivity to inhibitors[3,4]. MAO enzymes[5] play a key role in the metabolism of monoamine neurotransmitters, and have been therefore studied in a number of psychiatric and neurological diseases[6]. Moreover, the MAO catalysed oxidative deamination of amines leads to the formation of hydrogen peroxide which is co-responsible for neurodegeneration[7]. Not surprisingly a number of MAO inhibitors have been investigated as neuroprotective agents in the treatment of Parkinson and Alzheimer diseases[3,4,6,8–10]. We have previously identified highly potent and selective MAO B inhibitors characterised by a 3,5-diaryl-4,5-dihydro-(1H)-pyrazole scaffold[11] and investigated on the structural requirements for the enzyme inhibition (Figure 1). In particular, the presence of two aryl substituents on the dihydro-(1H)-pyrazole nucleus appeared as essential for MAO B selectivity and inhibition potency activity[12–15]. Hence, we designed and studied 2-thiazolylhydrazones derivatives, ideally originated by removing C4 and C5 from the dihydropyrazole ring. These derivatives exhibited high potency and selectivity towards MAO B[16–19]. More recently, through the isosteric replacement of the carbon 4 of the previously reported dihydropyrazole derivatives[11] with an oxygen atom, we have designed and synthesised two series of 2,3-dihydro-oxadiazoles[20–22] that exhibited high selectivity and activity towards MAO B. Moreover, we observed that the introduction of a 3,4-dichlorophenyl substituent in the position 2 of the dihydro-oxadiazole core is crucial for both selectivity and potency[21]. According to these structural information and with the aim of setting new hit structures for MAO B inhibition, we have devised a synthetic pathway to obtain 3,5-diaryl-4,5-dihydroisoxazoles as bio-isosters of both the previously reported 3,5-diaryl-4,5-dihydro-(1*H*)-pyrazoles and 2,5-diaryl-2,3-dihydro-1,3,4-oxadiazoles.

Methods

Materials and apparatus

Starting materials and reagents were obtained from commercial suppliers and were used without purification. All melting points were determined on a Stuart SMP11 melting points apparatus and are uncorrected (East Yorkshire, UK). Electron ionization mass spectra were obtained by a Fisons QMD 1000 mass spectrometer (70 eV, 200 mA, ion source temperature 200 °C) (Loughborough, UK). Samples were directly introduced into the ion source. Found mass values are in agreement with theoretical ones. Melting points, yield of reactions and the analytical and descriptive data of derivatives are reported in Table 1.

^{1}H-NMR (Table 2) were registered on a Bruker AMX 300 MHz spectrometer (Billerica, MA). All samples were measured in $CDCl_3$. Chemical shifts are reported referenced to the solvent in which they were measured. Coupling constants *J* are expressed in Hz. Elemental analyses were obtained on a Perkin-Elmer 240 B microanalyser (Waltham, MA). Analytical data of the synthesised compounds are in agreement within ±0.4% of the theoretical values.

CONTACT Elias Maccioni maccione@unica.it Department of Life and Environmental Sciences, University of Cagliari, Via Ospedale 72, Cagliari 09124, Italy

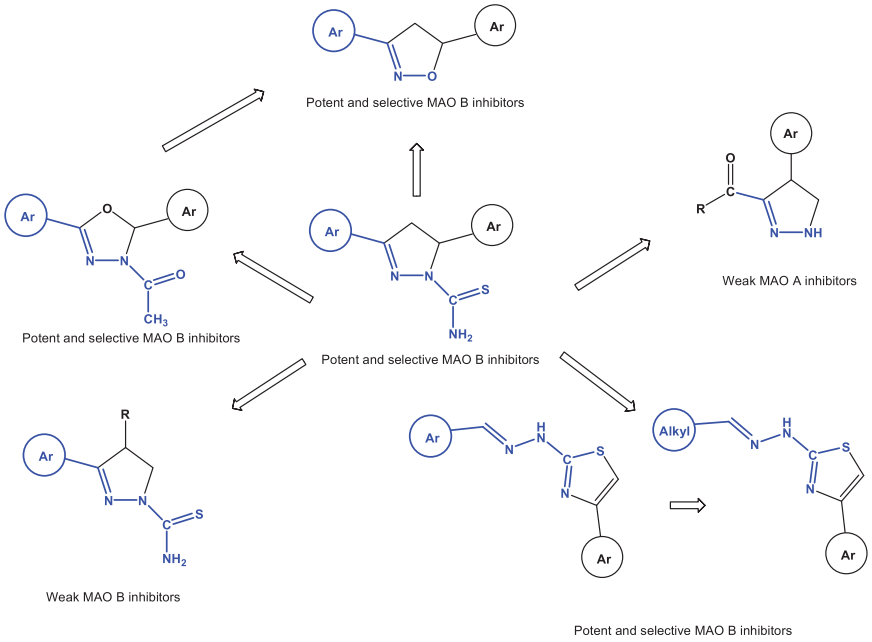

Figure 1. Scaffold evolution of MAO B inhibitors: from dihydro-pyrazoles to dihydro-isoxazoles.

Table 1. Chemical, analytical, and physical data of derivatives **EMAC II (i–m)**.

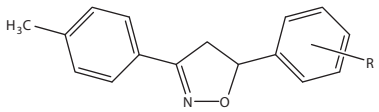

			C–H–N				
Compound	R	Cryst. solvent	Calc.	Found	M.P. (°C)	Yield %	E.I. 70 eV mass spectra *m/z* (rel. ab.)
EMAC II i	4-Cl	Ethanol	70.72, 5.19, 5.15	70.67, 5.17, 5.12	134-5	42	271 (100); 240 (78); 139 (17)
EMAC II j	4-CH_3	Ethanol	81.24, 6.82, 5.57	81.27, 6.83, 5.54	103-4	46	251 (100); 220 (83); 119 (13)
EMAC II k	4-F	Ethanol	75.28, 5.53, 5.49	75.31, 5.54, 5.43	132-4	41	255 (100); 224 (75); 123 (19)
EMAC II l	3,4-Cl	Water/ethanol	62.76, 4.28, 4.57	62.72, 4.31, 4.54	134-5	65	305 (100); 274 (81); 173 (22)
EMAC II m	4-OCH_3	ethanol	76.38, 6.41, 5.24	76.33, 6.40, 5.22	131-3	44	267 (100); 236 (71); 135 (9)

Table 2. ^{1}H NMR data and main fragments in E.I. mass spectrometry of derivatives **EMAC II (i–m)**.

Compound	^{1}**H NMR** δ (ppm)
EMAC II i	^{1}H-NMR: (300 MHz, $CDCl_3$) δH 2.38 (s, 3H, CH_3), 3.23 (dd, 1H, Jab 16.5, Jax 7.8, CH_2, isoxazole), 3.76 (dd, 1H, Jab 16.5, Jbx 10.1, CH_2, isoxazole), 5.59 (dd, 1H, Jbx 10.8, Jax 8.1, CH, isoxazole), 7.21 (d, 2H, J 7.8, CH, arom.), 7.33 (m, 4H, CH, arom.), 7.57 (2H, d, J 8.1, CH, arom.).
EMAC II j	^{1}H-NMR: (300 MHz, $CDCl_3$) δH 2.37 (s, 3H, CH_3), 2.43 (s, 3H, CH_3), 3.30 (dd, 1H, Jab 16.5, Jax 8.3, CH_2, isoxazole), 3.72 (dd, 1H, Jab 16.5, Jbx 10.8, CH_2, isoxazole), 5.66 (dd, 1H, Jbx 10.8, Jax 8.3, CH, isoxazole), 7.16–7.29 (m, 6H, CH, arom.), 7.57 (d, 2H, J 8.3, CH, arom.).
EMAC II k	^{1}H-NMR: (300 MHz, $CDCl_3$) δH 2.35 (s, 3H, CH_3), 3.27 (dd, 1H, Jab 16.7, Jax 8.0, CH_2, isoxazole), 3.74 (dd, 1H, Jab 16.5, Jbx 10.7, CH_2, isoxazole), 5.69 (dd, 1H, Jbx 10.7, Jax 8.3, CH, isoxazole), 7.04 (t, 2H, J 8.3, CH, arom.), 7.21 (d, 2H, J 8.1, CH, 4-CH_3-phenyl), 7.36 (dd, 2H, CH, J 8.3/5.3, arom.), 7.56 (d, 2H, J 8.2, CH, 4-CH_3-phenyl).
EMAC II l	^{1}H-NMR: (300 MHz, $CDCl_3$) δH 2.38 (s, 3H, CH_3), 3.27 (dd, 1H, Jab 16.7, Jax 7.8, CH_2, isoxazole), 3.78 (dd, 1H, Jab 16.4, Jbx 10.8, CH_2, isoxazole), 5.67 (dd, 1H, Jbx 10.8, Jax 7.8, CH, isoxazole), 7.21 (m, 3H, CH, arom.), 7.44 (d, 1H, J 8.2, CH, arom.), m, 7.49 (d, 1H, J 1.2, CH, arom.), 7.56 (d, 2H, J 8.1, CH, arom.).
EMAC II m	^{1}H-NMR: (300 MHz, $CDCl_3$) δH 2.38 (s, 3H, CH_3), 3.30 (dd, 1H, Jab 16.7, Jax 7.8, CH_2, isoxazole), 3.71 (dd, 1H, Jab 16.5, Jbx 10.6, CH_2, isoxazole), 3.80 (s, 3H, OCH_3), 5.66 (dd, 1H, Jbx 10.5, Jax 8.6, CH, isoxazole), 6.89 (d, 2H, J 8.3, CH, arom.), 7.21 (d, 2H, J 8.2, CH, 4-CH_3-phenyl), 7.31 (d, 2H, J 8.7, CH, arom.), 7.58 (d, 2H, J 8.2, CH, 4-CH_3-phenyl).

TLC chromatography was performed using silica gel plates (Merck F 254, Kenilworth, NJ), spots were visualised by UV light.

General procedure for the synthesis of compound derivatives

In a typical experiment, 0.0038 mol of the appropriate α,β-unsaturated ketone is dissolved in 30 ml of boiling absolute ethanol. On this solution, 10 ml of a freshly prepared hydroxylamine hydrochloride (0.0057 mol) and potassium hydroxide (0.013 mol) water solution are added dropwise. The solution becomes progressively orange and the reaction is monitored by thin layer chromatography (TLC) (CH_2Cl_2/n-hexane: 20/1). By cooling the reaction, the formation of a precipitate is observed which was filtered and crystallised from ethanol.

By this procedure (Scheme 1), compounds **EMAC II (i–m)** were synthesised.

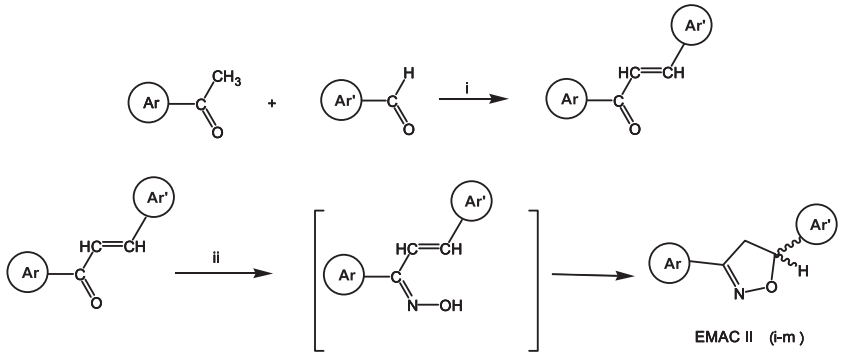

Scheme 1. Synthesis of **EMAC II (i–m)** compounds. Reagents and conditions: (i) ethanol, NaOH; (ii) ethanol, hydroxylamine hydrochloride, potassium hydroxide, reflux.

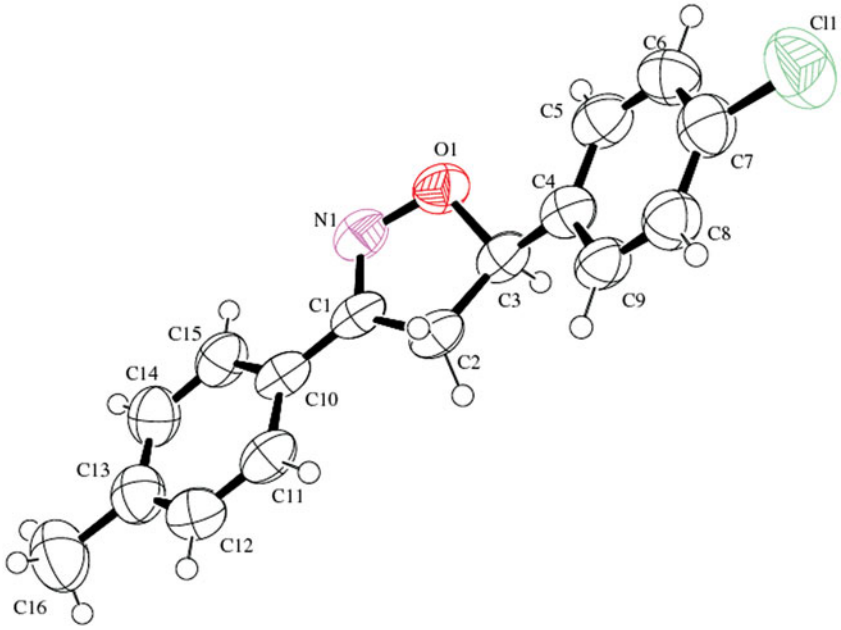

Figure 2. An ORTEP view of the molecular structure of (R)-(−)-**EMAC II i** enantiomer.

HPLC enantioseparations and stereochemical characterisation

Direct separation of the enantiomers of **EMAC II (i–m)** was achieved by HPLC using pure dichloromethane as the eluent. The resolving power of the immobilized-type was sufficiently high to achieve a baseline enantioseparation of all compounds in a short-time analysis. The optimized analytical conditions were easily scaled up to semipreparative level employing a 1 cm i.d. IA column. An amount of <20 mg of racemic samples was resolved for each chromatographic run, and both enantiomers were collected with high enantiomeric purity. The stereochemical characterization of compounds **EMAC II (i–m)** was performed by CD correlation comparing the maximum and minimum of ellitipticity of the CD spectra of the isolated enantiomers of compound **EMAC II i** of known stereochemistry (Figure 2), as previously described by some of us[23]. Single enantiomers were resubmitted to biological assay.

Biological assay

The inhibitory activities of compounds **EMAC II (i–m)** on human recombinant MAO A and B isoforms, expressed in baculovirus infected BTI infected cells, as IC_{50}, are reported in Table 1. Tested compounds demonstrated no interference with the measurements, since they were unable to directly react with the Amplex Red reagent. The kinetic parameters of hMAO-A and hMAO-B were evaluated in the presence of different tyramine concentrations. In our experiments, hMAO-A displayed a Michaelis constant (Km) of 514 ± 46.8 mM and a maximum reaction velocity (Vmax) of 301.4 ± 27.9 nmol/min/mg protein, whereas hMAO-B showed a Km of 104.7 ± 16.3 mM and a Vmax of 28.9 ± 6.3 nmol/min/mg protein ($n = 5$). Active compounds showed reversible behaviour according to the method proposed by Cer et al.[24] Hence, reported IC_{50} is a useful tool to determine the relative activity of the compounds within the series as well as to determine substituent and key positions in the scaffold. All the tested compounds exhibited inhibitory activity towards hMAO-B at nM concentration. Single enantiomers activity was evaluated indicating that stereochemistry plays a relevant role in determining inhibitory concentrations. None of the tested compounds exhibited activity towards the A isoform of the enzyme at the tested concentration of 100 μM.

Coordination studies

The interaction between **EMAC II l** and the Fe^{2+} or Fe^{3+} ions was evaluated by recording the UV/VIS absorbance spectra of **EMAC II l** (Figure 3) in absence and in presence either of $FeCl_3$ or $FeSO_4$. **EMAC II l** was solubilised in DMSO then diluted to 1 mM in

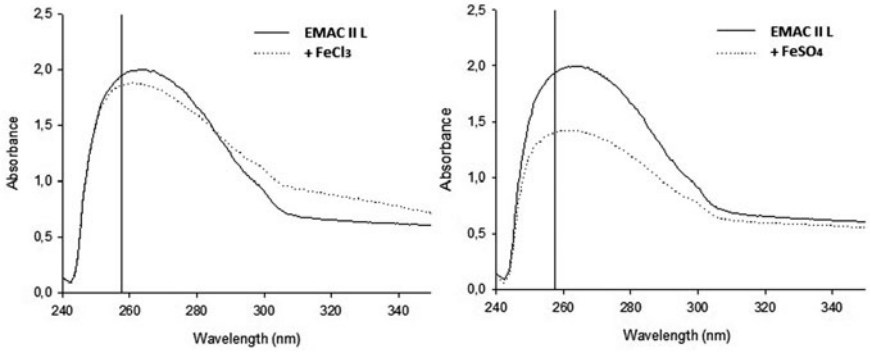

Figure 3. Effect of Fe^{2+} or Fe^{3+} ions on the spectrum of absorbance of **EMAC II l**. UV/vis spectrum was measured with 100 μM of compound alone (unbroken line) or in the presence of 10 mM $FeCl_3$ or $FeSO_4$ (dotted line).

Table 3. Inhibitory activities towards hMAO-A and hMAO-B of **EMAC II (i–m)** derivatives.

Compound	Structure	MAO-A (IC_{50})	MAO-B (IC_{50})	Ratio[e]
EMAC II i	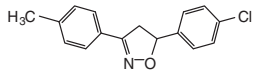	[b]	104.04 ± 3.69 nM	>961[d]
EMAC II j	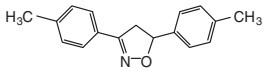	[b]	41.05 ± 1.52 nM	>2436[d]
EMAC II k	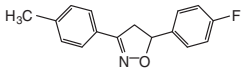	[b]	320.22 ± 13.61 nM	>312[d]
EMAC II l	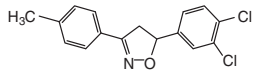	[b]	11.97 ± 0.37 nM	>8354[d]
EMAC II m	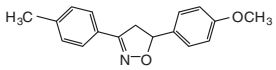	[b]	449.57 ± 18.02 nM	>222[d]
Clorgiline		4.46 ± 0.32 nM[c]	61.35 ± 1.13 μM	0.000073
L-Deprenyl		67.25 ± 1.02 μM[c]	19.60 ± 0.86 nM	3431.12
Iproniazide		6.56 ± 0.76 μM	7.54 ± 0.36 μM	0.87
Moclobemide		361.38 ± 19.37 μM	[a]	<0.36[e]

[a]Inactive at 1 mM (highest concentration tested).
[b]Inactive at 100 μM (highest concentration tested). At higher concentration, the compounds precipitate.
[c]Results are mean ± SEM from five experiments. Level of statistical significance: [c]P <0.01 versus the corresponding IC_{50} values obtained against MAO-B, as determined by ANOVA/Dunnett's.
[d]Values obtained under the assumption that the corresponding IC_{50} against MAO-A is the highest concentration tested (100 μM).
[e]Selectivity ratios [IC_{50}(MAO-A)]/[IC_{50}(MAO-B)].

50%DMSO solution. The UV/vis spectrum of the solution was recorded before and after addition of 10 mM final concentration either of $FeCl_3$ or $FeSO_4$. The spectra were recorded with a Ultrospec 2100 pro (Amersham Biosciences, Little Chalfont, UK) and analysed with SWIFT II-METHOD software (GE Healthcare, Little Chalfont, UK).

Molecular modelling studies

Protein preparation. Three-dimensional coordinates of the receptor[25] were obtained from the Protein Data Bank (PDB).[26] The protein was processed and the internal hydrogen bonding network of the receptor was optimized using the algorithm implemented in Protein Preparation wizard.[27]

Ligand preparation. The ligands were built using Maestro GUI[27]. The lowest energy conformer was considered for the subsequent computational studies. This was obtained with MacroModel version 7.2[28], considering MMFFs[29] as force field and solvent effects by adopting the implicit solvation model Generalized Born/Surface Area (GB/SA) water[30]. The simulation was performed allowing 1000 steps Monte Carlo analysis with Polak-Ribier Conjugate Gradient (PRCG) method and a convergence criterion of 0.05 kcal/(mol Å).

Docking experiments. Previous reported and validated QMPL docking protocol was applied using default settings[21,31]. In order to better take into account the induced fit phenomena, the most energy favoured generated complexes were fully optimized with the AMBER* united atoms force field[32] in GB/SA implicit water,[30] setting 5000 steps iterations analysis with PRCG method and a convergence criterion of 0.1 kcal/(mol Å). Analysis of the results of the complex minimization was carried out taking into account the state equations (free energy of complex formation) computed at 300 K, applying molecular mechanics and continuum solvation models with the molecular mechanics generalized Born[33]. The resulting complexes were considered for the binding modes graphical analysis with Pymol[34] and Maestro[27].

Results and discussion

Pursuing in our research on the design and synthesis of new agents for the selective inhibition of MAO B, we have synthesised a series of 3,5-diaryl-4,5-dihydro-isoxazoles **EMAC II (i–m)**. All the

compounds were submitted to biological evaluation to investigate their ability to inhibit both MAO isoforms. The structure and the MAO A and MAO B IC_{50} values and selectivity ratios of the new derivatives are reported in Table 3. All the compounds inhibit MAO B isozyme with IC_{50} values ranging from higher to lower nanomolar range. Accordingly to what is observed in our previous report on similar derivatives[21], compound **EMAC II l**, bearing a 3,4-dichlorophenyl moiety in the position 5 of the dihydro-isoxazole ring resulted, the most active within all the tested compounds. Based on this observation we assumed that, in the formation of the enzyme–ligand complex, this portion of the inhibitor is, in all probability, oriented similarly with respect to our previously reported compounds. Interestingly, none of the new compounds exhibited activity towards the MAO A isoform of the enzyme up to 100 μM concentration. Considering the presence of an asymmetric carbon at the position 5 of the dihydro-isoxazole nucleus we performed, semipreparative chromatographic enantio-separation of all the new derivatives **EMAC II (i–m)**. The separated enantiomers were then submitted to biological evaluation (Table 4). The obtained data pointed out the importance of enantiomeric separation for both potency and selectivity. In particular, in the case of compound **R-(−)-EMAC II l**, the IC_{50} value towards MAO B, drops from 11.97 nM to 1.89 nM, while the selectivity towards MAO B is increased by more than six folds. Moreover, considering the growing interest in the development of iron chelators for the treatment of neurodegenerative disorders[35–37], we have preliminarily investigated our best compound able to bind iron II and iron III cations following a previously reported procedure[38]. According to our preliminary results (Figure 3), compound **EMAC II l** do not have the ability to bind neither iron II nor iron III cations.

In order to explore the nature of the ligand–receptor interactions, we have carried out docking experiments considering the MAO B active site by means of QMPL docking protocol[31,39,40]. We have focused our attention on the most active compound **R-(−)-EMAC II l**, which shows the lowest IC_{50} value and the highest selectivity towards MAO-B.

It should be pointed out that MAO-B cavity is rather narrow, therefore, small changes are reflected in the biological activity. In this respect, the best compound shows remarkable difference of activity between the R and the S enantiomers. An analogous behaviour was observed in the previous series[11,20]. According to docking and post docking best scored pose, the most stable complex configurations of both R and S enantiomers are depicted in Figure 4(a,b).

Table 4. Inhibitory activities towards hMAO-A and hMAO-B of **EMAC II (i–m)** single enantiomers.

Compound	MAO-A (IC_{50})	MAO-B (IC_{50})	Ratio
R-(−) EMAC II i	[a]	15.27 ± 0.95 nM	6549[b]
S-(+) EMAC II i	[a]	[a]	
R-(−) EMAC II j	[a]	2.55 ± 0.11 nM	39 216[b]
S-(+) EMAC II j	[a]	31.37 ± 1.67 μM	3188[b]
R-(−) EMAC II k	[a]	299.86 ± 12.04 nM	333.5[b]
S-(+) EMAC II k	[a]	33.82 ± 1.12 μM	2956[b]
R-(−) EMAC II l	[a]	1.89 ± 0.16 nM	52 910[b]
S-(+) EMAC II l	[a]	10.96 ± 0.83 μM	9124
R-(−) EMAC II m	[a]	126.16 ± 8.44 nM	792.6[b]
S-(+) EMAC II m	[a]	291.82 ± 13.45 nM	342.6

IC_{50} values are the mean ± SEM from five experiments.
[a]Inactive at 100 μM (highest concentration tested).
[b]Values obtained under the assumption that the corresponding IC_{50} against MAO-B is the highest concentration tested (100 μM).

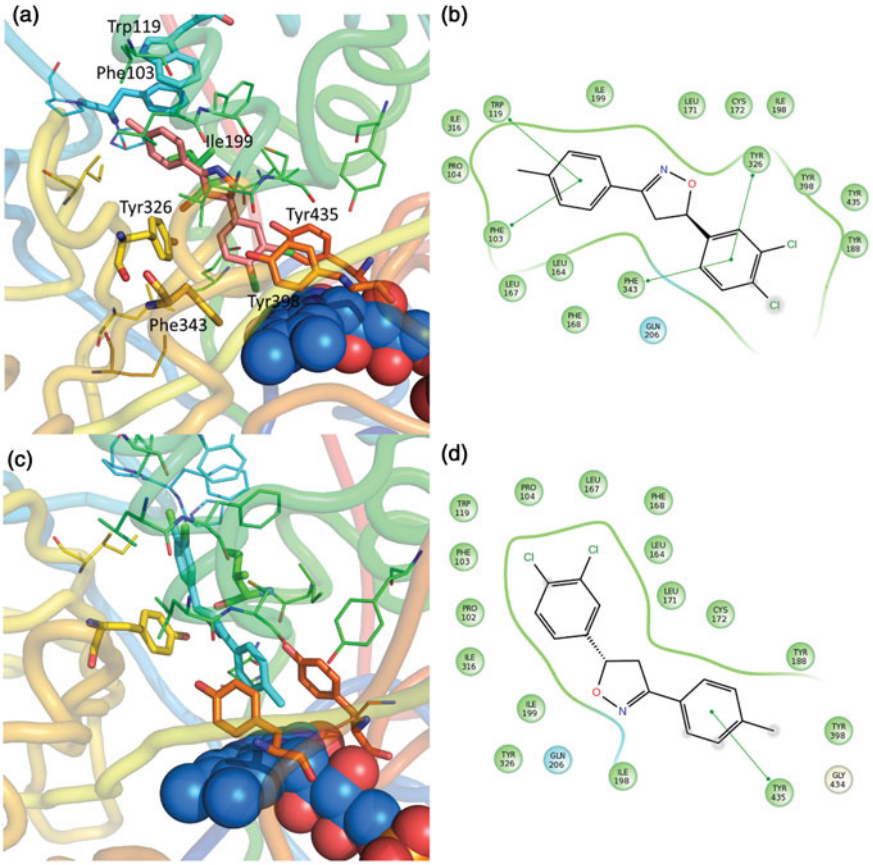

Figure 4. Putative binding mode of compound **EMAC II l**. (a) **R-(−)-EMAC II l**/MAO-B complex; (c) **S-(+)-EMAC II l**/MAO-B complex; (b, d) compound 2D representation and binding pocket interacting residues: green, hydrophobic; cyan, polar residues. Green arrows indicate π−π interactions.

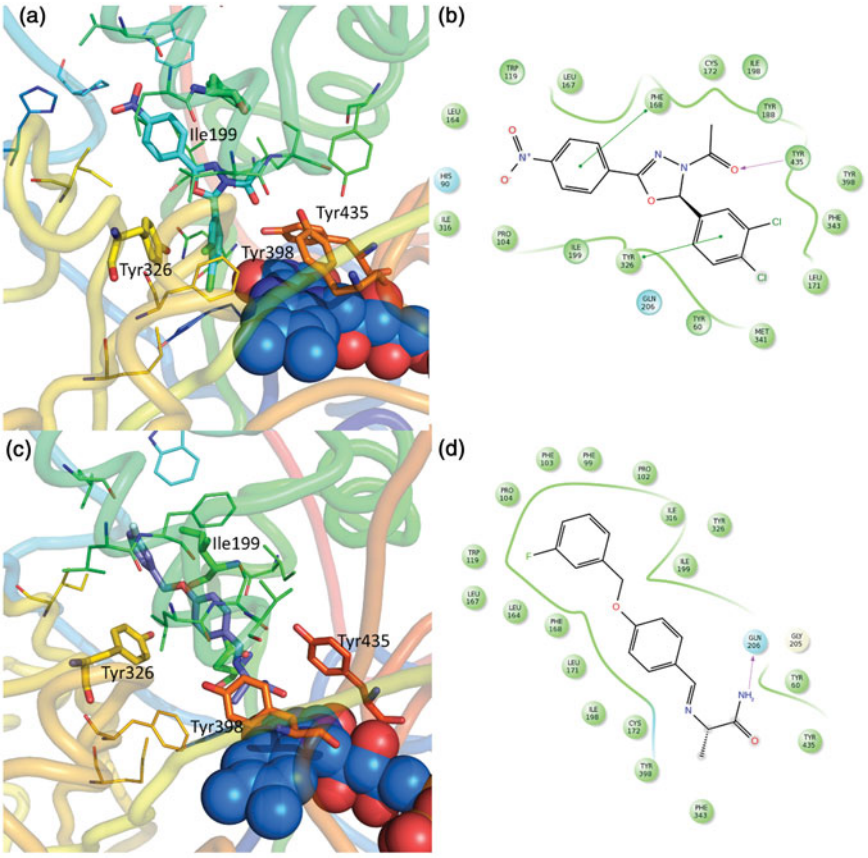

Figure 5. Binding mode of previously published compounds and approved inhibitors. (a) **4f-(R)** MAO-B complex[21]; (c) safinamide MAO-B complex (pdb code 4v5z)[25]; (b, d) compound 2D representation and binding pocket interacting residues: in green, hydrophobic; cyan, polar residues. Green arrows indicate $\pi-\pi$ interactions, magenta arrow indicates H bonds.

The *R* enantiomer is stabilized by $\pi-\pi$ interactions with Trp119, Phe103, Phe343, Tyr326 and some hydrophobic interactions with several residues in the binding pocket: Leu 164, Leu 167, Phe 168, Ile 316, Ile 199, Ile198, Leu 171 and the Tyr of the aromatic cage 435, 298, 188.

Conversely, the *S* enantiomer is oriented in the opposite way: with the dichlorophenyl substituent in the entrance cavity and the 4-methylphenyl substituent in the catalytic cavity toward the FAD. The complex results in less stability and gives rise only to a single $\pi-\pi$ interaction with Tyr 435 and several hydrophobic interactions (Figure 4(c,d)).

Compared with previous series[21], the absence of acetyl group allows a better accommodation in the cavity (Figures 4(a) and 5(a)). Once again, the importance in crossing both entrance and catalytic cavity, in order to achieve the MAO-B isoform selective activity is confirmed. This essential requisite has been reported by several studies[25,41,42] and can be observed in co-crystallized selective MAO B inhibitors. A typical example is the inhibitor safinamide (Figure 5(c,d))[25,43].

Conclusions

In summary, a small library of 3,5-diaryl-4,5-dihydroisoxazoles have been designed and synthesized on the basis of previously reported MAO inhibitors. Our finding highlighted the capability of 3,5-diaryl-4,5-dihydroisoxazoles to exert specific recognition and inhibition against the isoform B of MAO. The stereochemical characterization of *R/S* enantiomers confirms an enantioselective effect against MAO B isoform. This scaffold is definitively interesting for the development of novel selective neuroprotective agents.

Disclosure statement

The authors have no declarations of interest to report.

References

1. Singer TP, Von Korff RW, Murphy DL, eds. Monoamine oxidase: structure, function, and altered functions. [Papers from a Symposium Held at the Michigan Molecular Institute, Midland, on July 15–19, 1979]. Academic Press; 1979:557 pp.
2. Mure M, Mills SA, Klinman JP. Catalytic mechanism of the Topa quinone containing copper amine oxidases. Biochemistry 2002;41:9269–78.
3. Kumar B, Sheetal Mantha AK, Kumar V. Recent developments on the structure–activity relationship studies of MAO inhibitors and their role in different neurological disorders. RSC Adv 2016;6:42660–83.
4. Naoi M, Maruyama W, Inaba-Hasegawa K. Type A and B monoamine oxidase in age-related neurodegenerative disorders: their distinct roles in neuronal death and survival. Curr Top Med Chem (Sharjah, United Arab Emirates) 2012;12:2177–88.
5. Shih JC, Chen K, Ridd MJ. Monoamine oxidase: from genes to behavior. Annu Rev Neurosci 1999;22:197–217.
6. Kong P, Zhang B, Lei P, et al. Neuroprotection of MAO-B inhibitor and dopamine agonist in Parkinson disease. Int J Clin Exp Med 2015;8:431–9.
7. Jha SK, Jha NK, Kumar D, et al. Linking mitochondrial dysfunction, metabolic syndrome and stress signaling in neurodegeneration. Biochim Biophys Acta Mol Basis Dis 2016 [Epub ahead of print]. DOI: 10.1016/j.bbadis.2016.06.015.

8. Giladi N, Asgharnejad M, Bauer L, et al. Rotigotine in combination with the MAO-B inhibitor selegiline in early Parkinson's disease: a post hoc analysis. J Parkinsons Dis 2016;6:401–11.
9. Perez-Lloret S, Rascol O. The safety and efficacy of safinamide mesylate for the treatment of Parkinson's disease. Expert Rev Neurother 2016;16:245–58.
10. Wang Y, Sun Y, Guo Y, et al. Dual functional cholinesterase and MAO inhibitors for the treatment of Alzheimer's disease: synthesis, pharmacological analysis and molecular modeling of homoisoflavonoid derivatives. J Enzyme Inhib Med Chem 2016;31:389–97.
11. Chimenti F, Maccioni E, Secci D, et al. Synthesis, molecular modeling studies, and selective inhibitory activity against monoamine oxidase of 1-thiocarbamoyl-3,5-diaryl-4,5-dihydro-(1H)-pyrazole derivatives. J Med Chem 2005;48:7113–22.
12. Cardia MC, Sanna ML, Meleddu R, et al. A novel series of 3,4-disubstituted dihydropyrazoles. Synthesis and evaluation for MAO enzyme inhibition. J Heterocycl Chem 2013;50:E87–92.
13. Secci D, Carradori S, Bolasco A, et al. Discovery and optimization of pyrazoline derivatives as promising monoamine oxidase inhibitors. Curr Top Med Chem (Sharjah, United Arab Emirates) 2012;12:2240–57.
14. Maccioni E, Alcaro S, Orallo F, et al. Synthesis of new 3-aryl-4,5-dihydropyrazole-1-carbothioamide derivatives. An investigation on their ability to inhibit monoamine oxidase. Eur J Med Chem 2010;45:4490–8.
15. Carradori S, Silvestri R. New frontiers in selective human MAO-B inhibitors. J Med Chem 2015;58:6717–32.
16. Chimenti F, Maccioni E, Secci D, et al. Selective inhibitory activity against MAO and molecular modeling studies of 2-thiazolylhydrazone derivatives. J Med Chem 2007;50:707–12.
17. Chimenti F, Maccioni E, Secci D, et al. Synthesis, stereochemical identification, and selective inhibitory activity against human monoamine oxidase-B of 2-methylcyclohexylidene-(4-arylthiazol-2-yl)hydrazones. J Med Chem 2008;51:4874–80.
18. Chimenti F, Secci D, Bolasco A, et al. Synthesis, semipreparative HPLC separation, biological evaluation, and 3D-QSAR of hydrazothiazole derivatives as human monoamine oxidase B inhibitors. Bioorg Med Chem 2010;18:5063–70.
19. Distinto S, Yanez M, Alcaro S, et al. Synthesis and biological assessment of novel 2-thiazolylhydrazones and computational analysis of their recognition by monoamine oxidase B. Eur J Med Chem 2012;48:284–95.
20. Maccioni E, Alcaro S, Cirilli R, et al. 3-Acetyl-2,5-diaryl-2,3-dihydro-1,3,4-oxadiazoles: a new scaffold for the selective inhibition of monoamine oxidase B. J Med Chem 2011;54:6394–8.
21. Distinto S, Meleddu R, Yanez M, et al. Drug design, synthesis, in vitro and in silico evaluation of selective monoaminoxidase B inhibitors based on 3-acetyl-2-dichlorophenyl-5-aryl-2,3-dihydro-1,3,4-oxadiazole chemical scaffold. Eur J Med Chem 2016;108:542–52.
22. Cerioni G, Maccioni E, Cardia MC, et al. Characterization of 2,5-diaryl-1,3,4-oxadiazolines by multinuclear magnetic resonance and density functional theory calculations. Investigation on a case of very remote Hammett correlation. Magn Reson Chem 2009;47:727–33.
23. Sanna ML, Maccioni E, Vigo S, et al. Application of an immobilised amylose-based chiral stationary phase to the development of new monoamine oxidase B inhibitors. Talanta 2010;82:426–31.
24. Cer RZ, Mudunuri U, Stephens R, Lebeda FJ. IC50-to-Ki: a web-based tool for converting IC50 to Ki values for inhibitors of enzyme activity and ligand binding. Nucleic Acids Res 2009;37:W441–5.
25. Binda C, Wang J, Pisani L, et al. Structures of human monoamine oxidase B complexes with selective noncovalent inhibitors: safinamide and coumarin analogs. J Med Chem 2007;50:5848–52.
26. Berman HM, Westbrook J, Feng Z, et al. The Protein Data Bank. Nucleic Acids Res 2000;28:235–42.
27. Schrödinger LLC. Maestro GUI. New York (NY); 2015.
28. Mohamadi F, Richards NGJ, Guida WC, et al. Macromodel—an integrated software system for modeling organic and bioorganic molecules using molecular mechanics. J Comput Chem 1990;11:440–67.
29. Halgren T. Merck molecular force field. II. MMFF94 van der Waals and electrostatic parameters for intermolecular interactions. J Comput Chem 1996;17:520–52.
30. Still WC, Tempczyk A, Hawley RC, Hendrickson T. Semianalytical treatment of solvation for molecular mechanics and dynamics. J Am Chem Soc 1990;112:6127–9.
31. Schrödinger LLC. QMPolarized protocol. Schrodinger Suite. New York (NY); 2015.
32. McDonald DQ, Still WC. AMBER torsional parameters for the peptide backbone. Tetrahedron Lett 1992;33:7743–6.
33. Kollman PA, Massova I, Reyes C, et al. Calculating structures and free energies of complex molecules: combining molecular mechanics and continuum models. Acc Chem Res 2000;33:889–97.
34. PyMOL. Version 1.5.0.4. Molecular Graphics System. Schrödinger, LLC.
35. He X-f, Lan Y, Zhang Q, et al. Deferoxamine inhibits microglial activation, attenuates blood-brain barrier disruption, rescues dendritic damage, and improves spatial memory in a mouse model of microhemorrhages. J Neurochem 2016;138:436–47.
36. Dexter DT, Statton SA, Whitmore C, et al. Clinically available iron chelators induce neuroprotection in the 6-OHDA model of Parkinson's disease after peripheral administration. J Neural Transm (Vienna) 2011;118:223–31.
37. Santos MA, Chand K, Chaves S. Recent progress in multifunctional metal chelators as potential drugs for Alzheimer's disease. Coord Chem Rev 2016;327–328:287–303.
38. Meleddu R, Distinto S, Corona A, et al. Exploring the thiazole scaffold for the identification of new agents for the treatment of fluconazole resistant Candida. J Enzym Inhibit Med Chem 2016;31:1672–7.
39. Cho AE, Guallar V, Berne BJ, Friesner R. Importance of accurate charges in molecular docking: quantum mechanical/molecular mechanical (QM/MM) approach. J Comput Chem 2005;26:915–31.
40. Chung JY, Hah J-M, Cho AE. Correlation between performance of QM/MM docking and simple classification of binding sites. J Chem Inform Model 2009;49:2382–7.
41. Binda C, Li M, Hubálek F, et al. Insights into the mode of inhibition of human mitochondrial monoamine oxidase B from high-resolution crystal structures. Proc Natl Acad Sci USA 2003;100:9750–5.
42. Edmondson DE, Binda C, Mattevi A. Structural insights into the mechanism of amine oxidation by monoamine oxidases A and B. Arch Biochem Biophys 2007;464:269–76.
43. Cattaneo C, Sardina M, Bonizzoni E. Safinamide as add-on therapy to levodopa in mid- to late-stage Parkinson's disease fluctuating patients: post hoc analyses of studies 016 and SETTLE. J Parkinsons Dis 2016;6:165–73.